Scalar Field Measurements in Reciprocating Engines

H. G. Green* and J. H. Whitelaw*
Imperial College of Science and Technology, London, England

Rayleigh scattering has been used to measure the mixing processes, resulting from the transient injection of freon gas, to simulate fuel, in a four-stroke model engine motored at 200 rpm with a compression ratio of 3.5. The effects of injector nozzle geometry have been investigated in detail and quantify the greater mixing achieved with a spray type nozzle than with diverging geometries.

Introduction

THE high-pressure, high-momentum, two-phase fuel injection process found in direct-injection diesel or stratified-charge engines is difficult to quantify even with the use of optical probes. Attempts to study the mixing of fuel and air have been limited and have usually made use of simulations of engine-flow environments, for example, Melton,[1] Witze,[2] Tanabe et al.,[3] and Tanaka,[4] or by injecting heavy gas jets into noncompressing low-speed engines, as in Arcoumanis et al.[5] The characterization of liquid sprays, and their atomization, has also been attempted, for example, by Kamimoto et al.,[6] Sinnamon et al.,[7] and Reitz and Bracco.[8]

In the present paper, a fuel spray has been simulated by a transient jet of freon-12 vapor injected through an axisymmetric valve into a model diesel engine motored at 200 rpm. The injection takes place near the end of the compression stroke and the subsequent mean and rms distributions of the freon concentration have been quantified using laser-induced Rayleigh scattering: the velocity characteristics of the flow, in the absence of the fuel jet, are known from the measurements of Vafidis.[9]

The experimental system and flow configurations are described in the next section. The third section discusses the results, and the more important conclusions are reported in the final section.

Experimental System

Flow Configuration

The operating characteristics of the plexiglass model engine are summarized in Table 1 and described in greater detail by Vafidis.[9] Freon-12 was chosen to simulate fuel because of its high density relative to air ($\rho_{freon}/\rho_{air} \sim 4.2$) and the large Rayleigh scattering cross section of freon-12 molecules relative to air ($\sigma_{freon}/\sigma_{air} = 17.9$); its density is similar to that of vaporized diesel oil. It was injected through a nozzle inserted in the center of a single axisymmetric valve, which was operated by a dual cam and rocker mechanism and used for both the intake and exhaust flow during the four-stroke engine cycle. Measurements were obtained with the three nozzles shown in Fig. 1. Control of the fuel injection and synchronization of all real-time information was carried out in the manner described by Green.[10]

Fuel injection and measurement were carried out in every second four-stroke cycle so as to avoid accumulation of freon-12 vapor. The injection characteristics are summarized in Table 2 and are similar to those of previous studies, e.g., those of Johnston[11] and Arcoumanis et al.[5] The injector system comprised a solenoid valve (Angar Model 008), a 3.2-mm-diam hole along the axis of the valve stem, and one of the three nozzles mounted flush with the valve face. The backpressure was maintained constant at 0.55 MPa and the injection time at 16.7 ms, corresponding to approximately 20 deg of crank angle. A gated laser velocimeter was used to determine the exit-plane velocities which, with injection into atmospheric air, were 37.7, 30.9, and 57.0 m/s with nozzles A, B, and C, respectively, and imply Reynolds numbers of 52,600, 48,200, and 23,400. With injection into the compressing engine, these values were reduced to approximately 17.5, 14.0, and 38.0 m/s, with corresponding Reynolds numbers of 81,800, 74,400, and 53,100; the in-cylinder mass of freon injected for nozzles A, B, and C was 45.6, 45.6, and 8.57 mg. Since the acoustic velocity for the freon was around 150 m/s, the nozzles did not choke.

The cylinder pressure associated with the 3.5 compression ratio reduces the jet exit momentum to around 0.55 of that at atmospheric pressure. The implications of reduced momentum for similar operating conditions (backpressure and injection timing as used at atmospheric conditions) are increases in mixing and spread of the jet equivalent to an upstream shift in its virtual origin. Reitz and Bracco[8] have reported similar effects with their injection of liquid jets into pressurized gas environments. The momentum of the present jets is slightly lower than that reported by Arcoumanis et al.,[5] but still higher than that of Johnston.[11]

Optical and Signal Processing Systems

A line diagram of the optical arrangement and signal instrumentation is shown in Fig. 2. An argon-ion laser was operated at 1 W and 488 nm and provided a beam that was vertically polarized with an exit diameter of approximately 1.5 mm. The beam was first expanded by a factor of three and passed through a half-wave retardation plate to rotate the plane of polarization to horizontal, and focused to a beam waist diameter of about 100 μm over a length of 1 mm with a 200-mm focal length lens L_1. The scattered light was collected with a 300-mm focal length lens L_2 over a solid angle of 0.071 sr normal to the observation volume and plane of polarization. The collected light was passed through a rectangular slit arrangement at the entrance to the photomultiplier (EMI 9816B); the dimensions of the slit defined an observation volume of 0.005 mm^3 based on the half-intensity diameter of the incident beam. Prior to entering the photomultiplier (PM) the light was optically filtered by a 10-nm interference filter and focused with a 25.4-mm-diam lens L_3 through a 50-μm pinhole. The anode current was converted to a voltage and input to a bandpass filter set at

Received Nov. 13, 1985; revision received Aug. 28, 1986.

*Mechanical Engineering Department, Fluids Section.

4-KHz cutoff. The signal was digitized at 30 KHz and sampled at a variable frequency (16 KHz max) with a microcomputer. The signal from a pressure transducer (Kistler Instruments 6121A1) was also input to the digitizing system and sampled simultaneously with the photomultiplier output. The uncertainty in the simultaneous measurement times was determined to be less than 2 μs. A third signal was obtained from an optical encoder, driven by the crank shaft, and was provided in the form of 1000 pulses per revolution with a marker pulse at top-dead-center (TDC) of compression.

Care was taken to ensure that the in-cylinder pressure at the start of injection, the engine speed, and the peak-cycle pressure were within predetermined tolerances for each cycle; the pressure tolerance was 0.001 MPa and the speed 1%. The ensemble averages were formed from around 4000 data at each measured location.

Sources of Error and Uncertainties

The sources of error in laser Rayleigh scattering (LRS) measurements have been documented in detail by Pitts and Kashiwagi;[12] additional sources in this application include variations in cylinder pressure and gas temperature. In addition, particles or droplets may give rise to scattered light which has to be distinguished from the molecular Rayleigh-scattered light.

For a binary mixture at constant temperature and pressure, a Rayleigh signal is based on variations in the effective (i.e., total mixture) Rayleigh scattering cross section and, thus, mole fraction. In the engine, the time-varying pressure requires that the signal be analyzed at the pressure at which scattering occurs. Calibration measurements under both static and time-varying conditions made with concentrations of freon-12 and air of 20, 40, 60, and 80% confirmed the expected linearity between pressure and intensity.

The static measurements were made with a pressure vessel having optical access while the time-varying results were obtained with the engine running. For the latter, the head was covered with a polyethylene bag and provision made for the intake gas to be varied. To ensure that the mixture concentration did not change, the scatter intensities before and after the running of the engine were determined and were found to be within $\pm 0.5\%$ of the expected values. Comparison of the static and time-varying results showed rms deviations of less than 1.5% and these were attributed to the sudden rise in gas temperature during compression which was small in the present case but may become important at higher compression ratios. An example of the time-varying calibration results is shown in Fig. 3.

Systematic checks were made during the measurements to ensure that the scatter intensity ratio between pure freon and air remained constant (16 ± 0.05). This ratio is slightly lower than the commonly reported value of 17.9 and due to impurities in the freon; note that $I_{freon}/I_{air} = \sigma_{freon}/\sigma_{air}$ where I_j is the detected Rayleigh-scatter intensity of the respective gases deconvoluted from noise.

Scattering from solid particles (e.g., room dust), was readily identified and removed when the intensity values were greater than that of pure freon. When particle scatter intensities fell below this maximum, the digital filtering tech-

Table 1 Characteristics of the model engine

Engine speed, rpm	200
Bore, mm	75.8
Stroke, mm	94
Connecting rod length, mm	363.5
Intake-exhaust valve	
Diameter, mm	33
Seat angle, deg	45
Flat piston	
Diameter, mm	75
Clearance at TDC, mm	36
Compression ratio	3.5
Piston bowl configuration	
Diameter, mm	49
Depth, mm	23
Compression ratio	3.2

Table 2 Injection characteristics

Injection pressure, MPa	0.55
Injection timing, deg BTDC	38
Injection duraction, deg	24

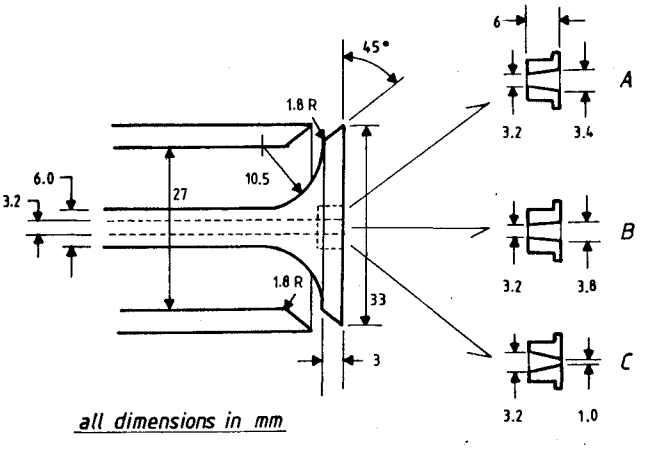

Fig. 1 Valve and freon jet arrangements.

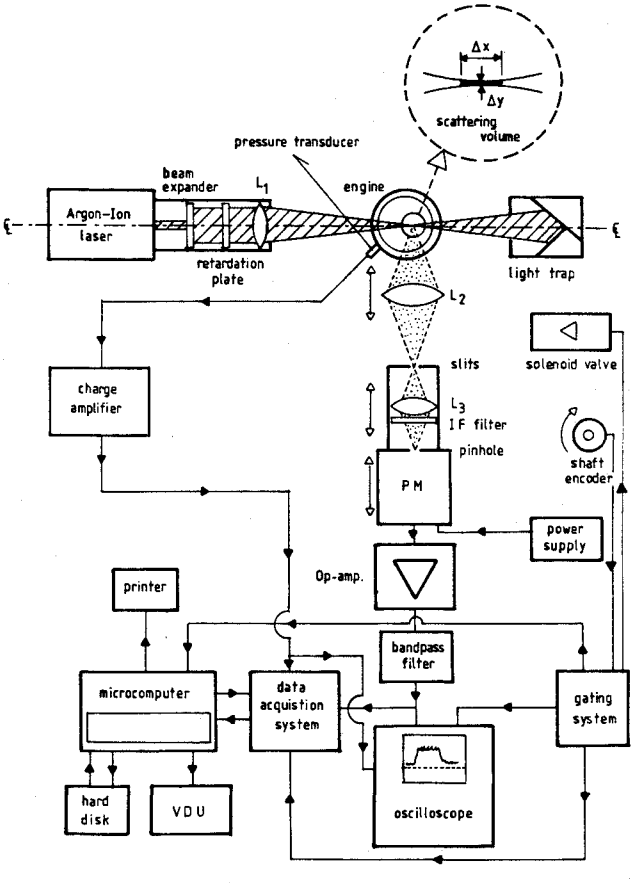

Fig. 2 Optical and signal processing arrangements.

Table 3 Influence of nozzle geometry on jet spread

Nozzle	x, mm	$r_{½}/d$
A	5	0.411
	10	0.867
	15	1.02
B	5	0.449
	15	1.03
C	5	0.650
	10	1.60
	15	1.85

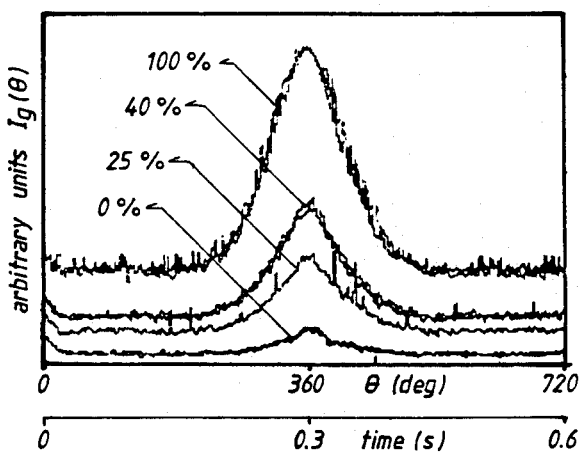

Fig. 3 Scattered light intensity as a function of pressure, concentration, and time.

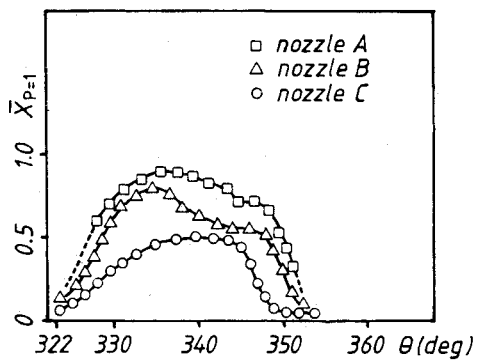

Fig. 4 Variations of ensembled-freon concentration reduced to atmospheric pressure (actual mole fraction): $x=5$ mm, $r/d=0$, flat piston.

niques described by Green[13] were used and resulted in a mean uncertainty of around 1.5% and about 3% for the rms.

The measured pressure-influenced signal intensities were corrected to atmospheric value according to the equation

$$I_g(\theta)=\frac{[I_g(\theta,P)-I_B]}{P} \tag{1}$$

where $I_g(\theta)$ is the equivalent instantaneous gas mixture scatter intensity at 1 atm, I_B the averaged optical background at the measurement location (detected using helium), and P the absolute pressure at the crank angle θ. It was possible in most instances to set $I_B=0$. The transient temperature error, introduced into the measured pressure, is around 0.005 bar and can be combined with the overall uncertainty in the pressure measurements to give a maximum error in the quantified mole fraction of less than 1%, assuming that in-cycle

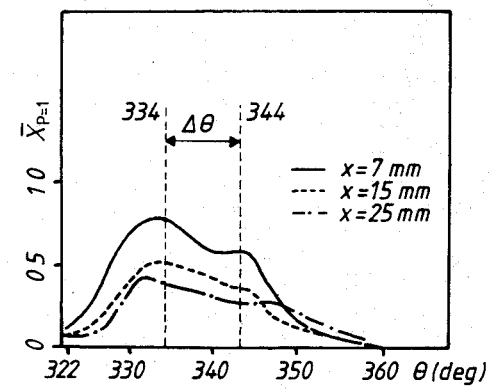

Fig. 5 Variations of ensembled-freon concentration for nozzle A: flat piston.

temperature effects are negligible. The more general form for the scatter intensity of the fuel/air mixture is given by

$$I_g=\frac{KP}{T}\Sigma X_i\sigma_i \tag{2}$$

(e.g., see Graham et al.[14]) where K is an experimental system constant, P and T the absolute pressure and temperature, X_i the mole fraction of the ith species, and σ_i the respective Rayleigh scattering cross sections. The ratio P/T defines the total number density N of molecules in the measurement volume, assuming ideal gas behavior or $N=\Sigma N_i\equiv P/T$.

The photon count rate N_p can be estimated from Eq. (2) (see, for example, Pitts and Kaskiwagi[12]) and results in the present case in 2×10^7 photons/s for air and 4.4×10^8 photons/s for freon-12. These values, along with the cutoff frequency $\Delta f=4$ KHz, define a signal-to-noise ratio $(\mathrm{SNR})=(N_p/2\Delta f)^{½}$ of about 233 or a relative uncertainty given by 1/(SNR) of 0.45%. For the pure air signal the relative uncertainty is about 2% and the corresponding SNR is 51. At the pressures of the measurements, the SNR values are improved by a factor of about $(P)^{½}$ and follow from Eq. (2) and the definition of the SNR; thus, the effects of photon statistics on higher statistical moments (i.e., variance, skewness, and kurtosis) are very small. Moreover, electronic shot-noise effects at pressures as found in the engine should be about 1%, but since the mole fractions are defined relative to atmospheric conditions [Eq. (1)], shot-noise uncertainty is more likely to be about 2%. Having obtained the corrected signal values for the Rayleigh scattering intensities $[I_g(\theta)]$, the mean mole fraction is related to the ensemble of the signal intensities by

$$\frac{X}{X_o}=\frac{I_g}{I_{go}} \tag{3}$$

where the subscript o refers to a reference state and the normalized rms intensity is given by

$$\frac{\bar{X}}{X_o}=\frac{(I_g'^2)^{½}}{I_{go}} \tag{4}$$

with $(I_g'^2)^{½}$ representing the rms of the signal after deconvolution of shot-noise effects and photon statistics (see Refs. 12 and 13). The results of the next section, as represented by Eqs. (3) and (4), have an estimated uncertainty in mean concentration of less than 3% in Eq. (3) with a maximum uncertainty in the rms of the concentration fluctuations of 7% in Eq. (4).

Results and Discussion

Results for the freon concentration field are presented in Figs. 4–11 in the form of concentration distributions and

centerline and radial profiles. The ensemble averaged in-cycle fuel concentrations for the three nozzles are shown in Fig. 4. These concentrations were obtained at the same axial location ($x=5$ mm) on the centerline and indicate the faster decay and mixing expected with the initially lower mass of injected fuel of nozzle C and the greater mixing of nozzle B relative to nozzle A, resulting from the increased diffusion angle of nozzle B. The decay in centerline concentration distributions with downstream distance is represented by Fig. 5. The results of Figs. 4 and 5 are based on instantaneous fuel-injection signals over 10^4 engine cycles, and examples for nozzle A at a centerline location of $x/d=2.47$ ($x=8.4$ mm) are shown in Fig. 6; both the pressure-influenced signal (Fig. 6a) and corrected signal (Fig. 6b) are shown. The start time of injection is consistent for each cycle, and the measured injection duration is effectively constant (16.7 ms).

The results of Fig. 6 may be compared with the noncompressing results of Fig. 7 and confirm that the penetration of the jet into compressed air is less than that in atmospheric air with increased jet decay and spread, as is expected from steady-flow results such as those of Green and Whitelaw.[15]

The spatial distributions of the mean and rms of the concentration fluctuations of Figs. 8–11 are based on ensemble averages over a 10-deg crank angle window $\Delta\theta$ centered at 21 deg before TDC. As can be seen from the downstream results indicated by Fig. 5, this averaging window consistently defines a region of characteristic behavior for the fuel-injection process. Averaging was also carried out with a 5-deg window centered at 21 deg before TDC, and comparison with the 10-deg results showed no differences. The choice of a 10-deg window improved the data acquisition rate and permitted more statistically accurate results to be obtained.

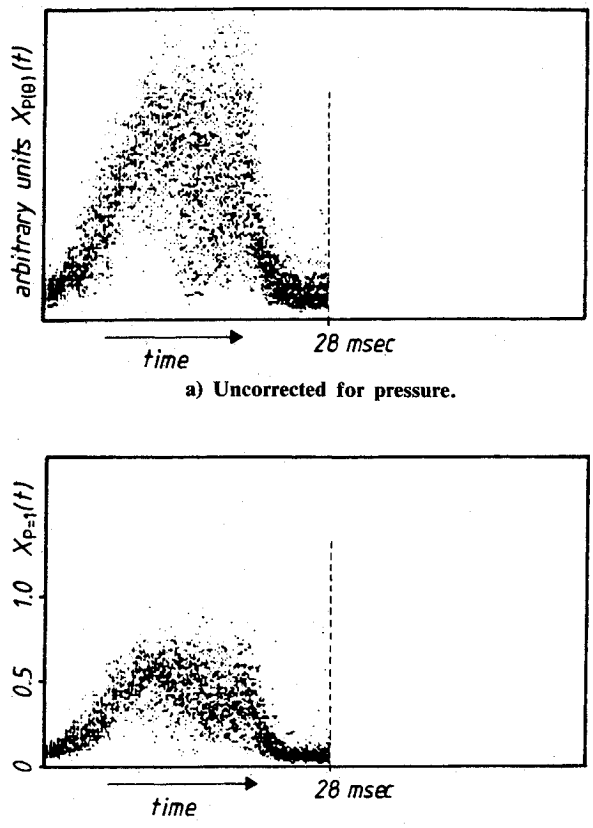

Fig. 6 Time-resolved variations of freon concentration: $x/d=2.47$, $r/d=0$, nozzle A, flat piston.

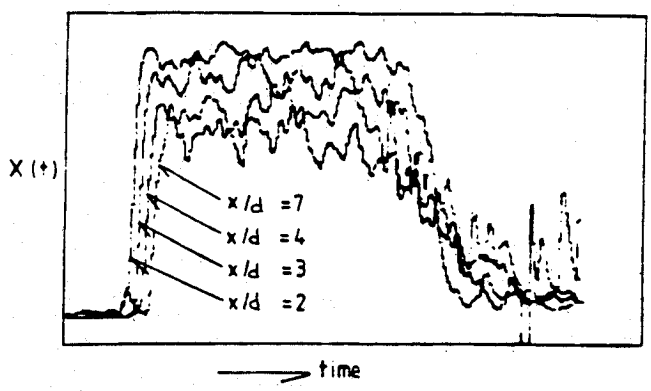

Fig. 7 Single traces of freon concentration: nozzle A in noncompressing engine.

Centerline Characteristics

In Fig. 8, results are presented for the mean and rms mole fraction concentration corresponding to the three nozzles with a flat piston and for nozzle A with a bowled-piston geometry; the mean values are normalized by the exit concentration X/X_o, where $X_o=1$ is the exit mole fraction. The mean concentration characteristics of Fig. 8a indicate results similar to those of free steady jets, where rapid initial decay of concentration is followed by a more gradual decay rate. The large distance represented by the ratio of piston clearance to nozzle diameter partly predicts that centerline concentration decay behavior similar to that found for free jets should exist. Similar observations have been made for the centerline velocity field of impinging jets as reported, for example, by Gutmark et al.[16] and Amano and Brandt.[17] Analysis of the results of Fig. 8a show that the initial decay of concentration for nozzle C is greatest, and that when the penetration distance is increased, as results with a bowled-piston, the initial decay is decreased, as indicated by the comparison of the results for nozzle A with a flat and bowled piston. Thus, a decrease in piston clearance leads to faster decay because of faster jet impingement onto the piston face. Further analysis shows that the downstream decay of the mean concentration is greater for the larger diffusing nozzles A and B than that which results for the convergent nozzle C. Comparison of these centerline results has been made by considering the reciprocal of the mean concentration of Fig. 8a, which can be described in terms of the well-known decay law $X_o/X=k(x-x_o)/r_o$ where k is a constant, x_o the virtual origin of the mole fraction, and r_o the nozzle radius. Often the effective nozzle radius is used to account for density differences when considering the mass fractions instead of mole fraction, for instance as in Refs. 12 and 15. Using the value of k determined for each case as a relative indication of the centerline decay rate, the values for nozzles A, B, and C (when a flat piston is used) are $k_A=0.120$, $k_B=0.114$, and $k_C=0.049$, and when the bowled-piston results are considered for nozzles A, $k_A=0.179$. Here, the larger the value of k, the larger the downstream decay rate implied. Toward the downstream region near the piston, the mean concentration levels for nozzles A and B become less dependent on upstream conditions. The concentration levels, however, remain higher for nozzles A and B because of the greater mass of fuel initially injected over nozzle C.

The rms distributions of Fig. 8b are presented in terms of the local rms divided by the local mean concentration $\bar{X}/X$; and this is referred to as "unmixedness."[12] As can be seen, the initial rise in $\bar{X}/X$ tends, with respect to the amount of mixing achieved, to an asymptotic behavior. The distance from the nozzle at which the asymptotic behavior begins to occur is influenced by the degree of mixing and the associated rate of concentration decay. It is observed that with nozzle C the lower mass of injected fuel, which is consequently more rapidly mixed with surrounding air, results in the fastest achievement of asymptotic behavior and lowest

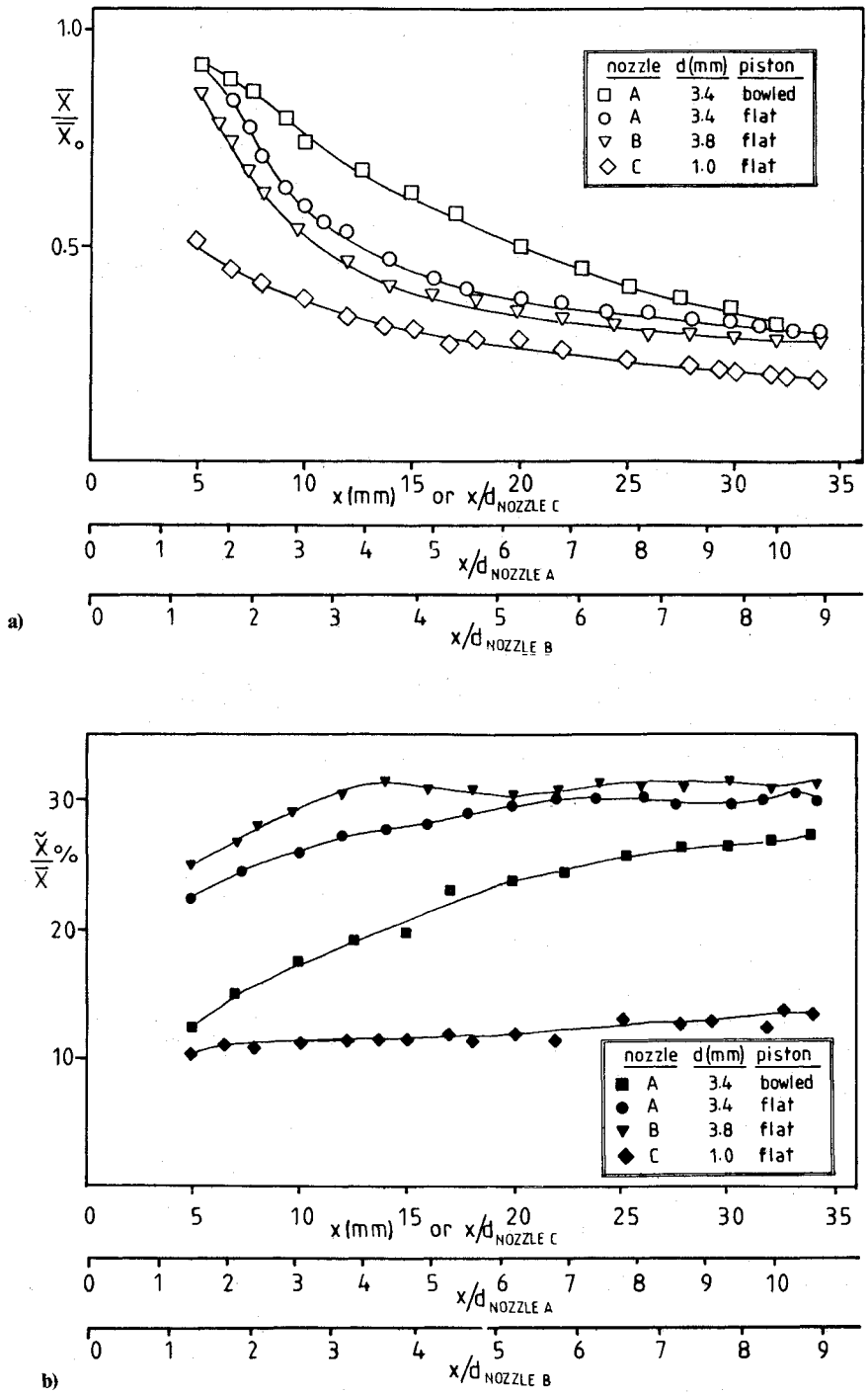

Fig. 8 Centerline distributions of ensemble-averaged mean and rms concentration.

levels of $\tilde{X}/X$. In contrast, the case of nozzle A with the bowled piston (which results in the slowest mixing due in part by the increased penetration distance) indicates a slower growth toward asymptotic behavior in the characteristics of $\tilde{X}/X$. Moreover, the increased spread and thus mixing of the fuel jet from nozzle B over nozzle A, resulting from the increased diffusing angle of nozzle B, also shows a consistent trend in the resulting behavior of $\tilde{X}/X$. Normalizing the local values of the rms $\tilde{X}$ by the exit mean mole fraction (i.e., $X_o = 1.0$) shows, as expected, that values of $\tilde{X}/X_o$ decrease with distance from the nozzle with values for nozzles A and B tending toward 9% rms and those for nozzle C to around 3%. These values suggest, when compared to similar results obtained in a noncompressing engine (Ref. 5), that the effect of compression through the increase of the in-cylinder air density results in decreased penetration of the fuel jet and increased mixing, particularly as lower values of $\tilde{X}/X_o$ resulting near the piston indicate a more homogeneous air/fuel mixture.

Radial Characteristics

Radial profiles of mean and rms concentration for nozzles A, B, and C, obtained with a flat piston, are shown in Figs. 9–11, respectively. The mean radial distributions are normalized by the centerline value of concentration. These radial profiles show that the rate of decay $\partial X/\partial r$ decreases with downstream distance, as indicated by the broadening of mean profiles, and is consistent with the variations in the mole fraction close to the cylinder axis. The rms quantities tend toward a maximum and then decrease with the ratio $\tilde{X}_{max}/\bar{X}_{CL}$ not ex-

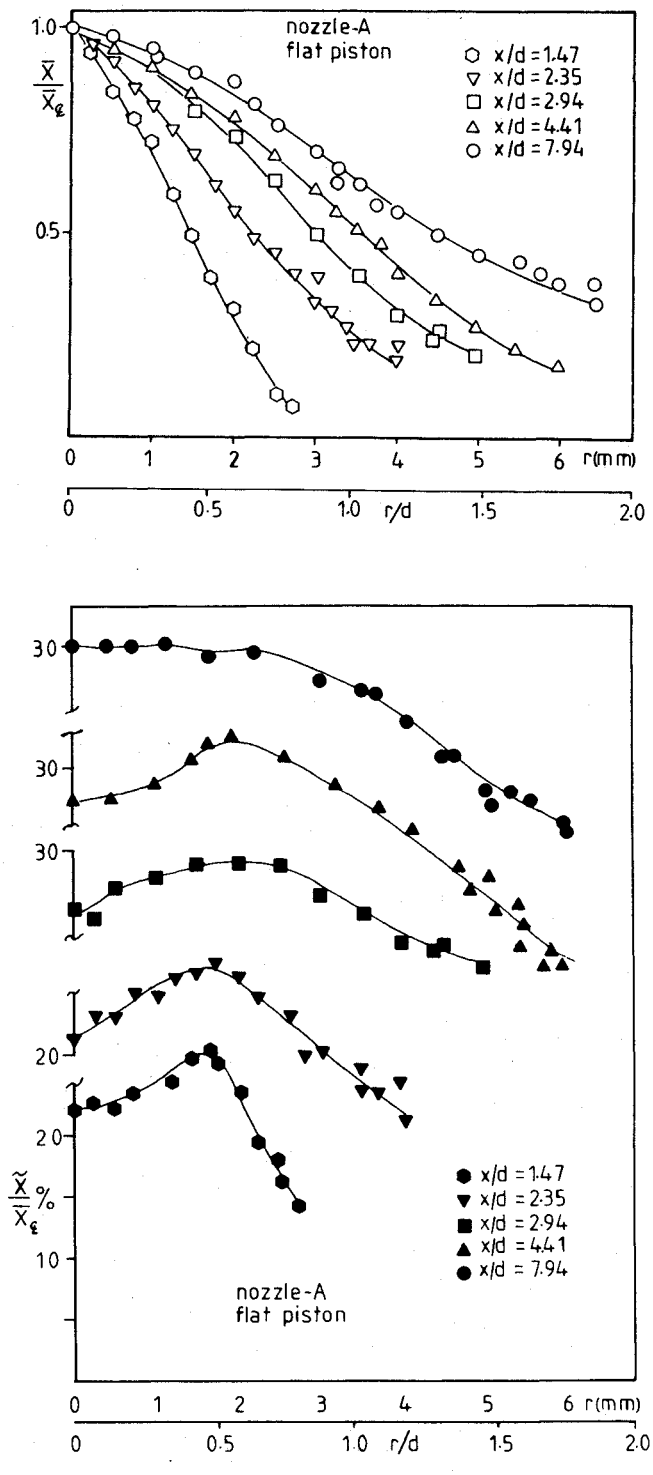

Fig. 9 Profiles of ensemble-averaged mean and rms concentration: nozzle A, flat piston.

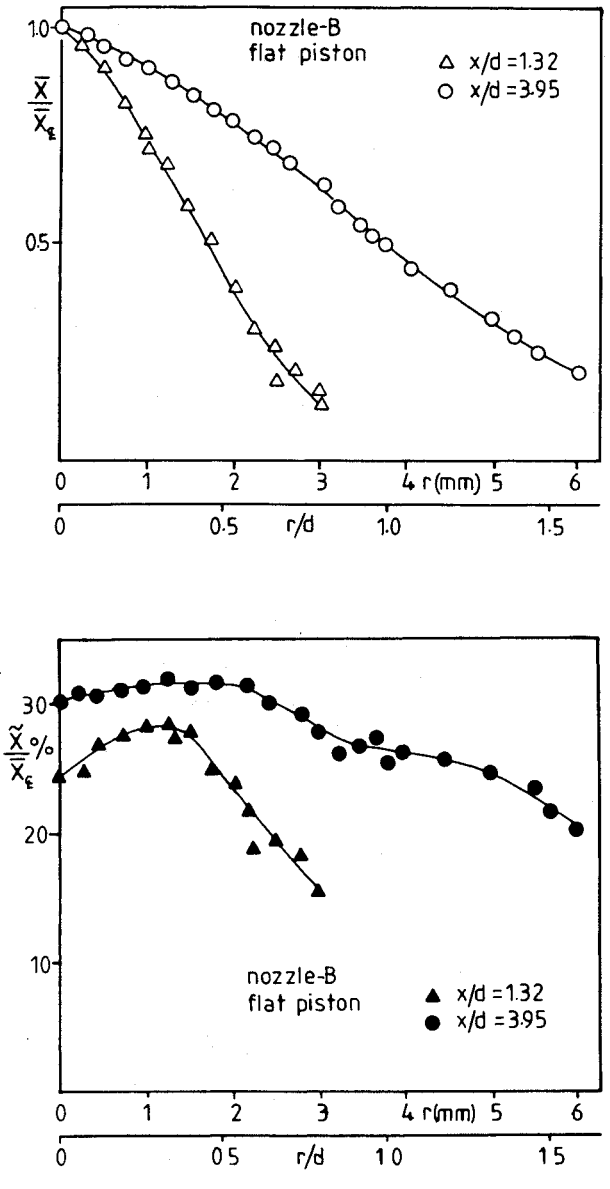

Fig. 10 Profiles of ensemble-averaged mean and rms concentration: nozzle B, flat piston.

ceeding 1.15, although in steady jets this ratio can be as high as 1.35 for jets having a density less than the surroundings and around 1.07 for jets of heavier density than the surroundings. The present results indicate that the combined reduction in the jet to surrounding air density ratio (caused by the compression process) and the transient characteristics of the fuel jets result in more intensive mixing for an initially heavy density fuel jet. In addition, examination of the probability density distributions (pdf) of the ensembled values of the mole fraction showed that they were skewed toward the lower values in a manner consistent with pdf's for the velocity characteristics of steady jets or the concentration characteristics of the steady jet of Green and Whitelaw.[15] The larger diffusing angle of nozzle B over nozzle A results in greater spread for nozzle B, which associates itself with the increased mixing evident in the results of Fig. 8. Thus, reduced spread rates result downstream as indicated by values of the constant k for nozzles A and B. Note that with nozzles A and B the same mass of fuel is injected.

When the results for the mean radial concentration of Figs. 9–11 are considered in terms of the radial coordinate $r/r_{1/2}$, with $r_{1/2}$ the radial location where the concentration falls to half of its centerline value, all the results tend to collapse on a single curve, which agrees well with the classical Gaussian distribution reported for similarity of steady jets, namely,

$$X/X_{CL} = \exp[-k'(r/r_{1/2})^2] \tag{5}$$

where $k' = \ell n\, 2$. For the radial rms distributions, a similarity collapse of the data does not result.

When the radial coordinate is made nondimensional by the nozzle diameter as r/d, the radial profiles of Figs. 9–11 indicate more clearly the extent to which the spreading rate differs for the different nozzles and the degree of mixing for each as indicated by levels of $\tilde{X}/X_{CL}$. These observations are consistent with the discussions of the centerline characteristics.

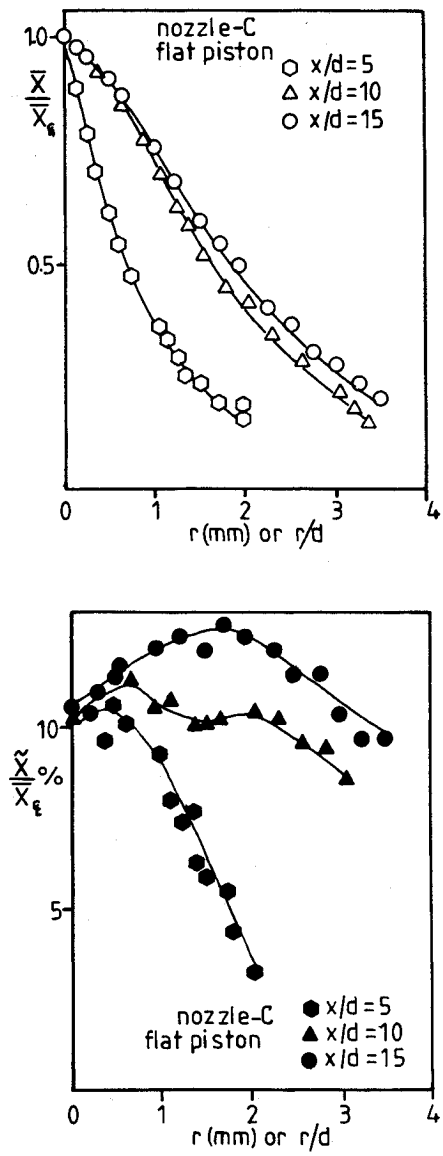

Fig. 11 Profiles of ensemble-averaged mean and rms concentration: nozzle C, flat piston.

An assessment of the influence of nozzle geometry on spreading is summarized in Table 3, which indicates a characteristic spread parameter $r_{1/2}/d$ for results obtained at the same axial locations within the cylinder with the different nozzles. The results show that the convergent (spray type) nozzle C gives rise to a characteristic spread $r_{1/2}/d$ of the order of 1.8 times greater than the diverging nozzles A and B and this is consistent with the more uniform air/fuel mixture implied by the centerline results of nozzle C over those of nozzles A and B. These relative quantitative features are well represented by the qualitative studies reported by Reitz and Bracco[8] in their studies of steady liquid jets used to simulate high-pressure diesel sprays.

Conclusions

The present investigation of the in-cylinder concentration field of a simulated fuel, in a model diesel engine operated in a four-stroke cycle with compression and motored a 200 rpm, revealed the following:

1) Injection of fuel into compressed air results in a more rapid decrease in jet momentum and in faster decay and increased mixing of the transient fuel jet, relative to the injection into atmospheric air.

2) The flowfield was found to be strongly dependent on the nozzle geometry. The convergent (spray type) nozzle showed a substantial departure from the characteristics of the diverging nozzles and gave rise to a greater characteristic spread over the diffusing nozzles.

3) The radial distributions of mean concentration showed similarity for all the nozzles when the radial coordinate is appropriately scaled.

4) The rate at which asymptotic behavior is approached for the centerline unmixedness was strongly influenced by the degree of air/fuel mixing resulting near the nozzle exit. Rapidly mixed air with injected fuel leads to the fastest development of asymptotic centerline characteristics indicative of homogeneous mixtures.

Acknowledgments

The authors gratefully acknowledge financial support from the Science and Engineering Research Council of the United Kingdom and the Department of Energy of the United States. They would also like to thank H. Wong for her assistance during the latter part of the work and C. Vafidis for his assistance. We are also grateful to J.R. Laker and N. Frost for their technical support.

References

[1]Melton, R.B., "Diesel Fuel Injection Viewed as a Jet Phenomenon," SAE Paper 710132, 1971.

[2]Witze, P.O., "The Impulsively Started Incompressible Jet," Sandia National Laboratories, Albuquerque, NM, SAND 80-8617, 1980.

[3]Tanabe, H., Ohnishi, M., Fujimoto, H., and Sato, G.T., "Experimental Study of the Transient Hydrogen Jet Using a Fast Response Probe," *International Journal of Hydrogen Energy,* Vol. 7, 1982, pp. 967-976.

[4]Tanaka, Y., "On the Structure of Pulse Jet," *Bulletin JSME,* Vol. 27, 1984, pp. 1667-1674.

[5]Arcoumanis, C., Green, H.G., and Whitelaw, J.H., "Velocity and Concentration Characteristics in Reciprocating Engines," *Experiments in Fluids,* Vol. 3, 1985. pp. 270-276.

[6]Kamimoto, T., Aoyagi, Y., Matsui, Y., and Matsuoka, S., "The Effects of Some Engine Variables on Measured Rates of Air Entrainment and Heat Release in a DI Diesel Engine," SAE Paper 800253.

[7]Sinnamon, J.F. Lancaster, D.R., and Steiner, J.C., "An Experimental and Analytical Study of Engine Fuel Spray Trajectories," SAE Paper 800135.

[8]Reitz, R.D. and Bracco, F.V., "Mechanism of Atomisation of a Liquid Jet," *Physics of Fluids,* Vol. 25, 1982, pp. 1730-1742.

[9]Vafidis, C., "Influence of Induction Swirl and Piston Configuration on Air Flow in a Four-Stroke Model Engine," *Proceedings of the Institution of Mechanical Engineers,* Vol. 198C, 1982, pp. 71-79.

[10]Green, H.G., "Development of Microcomputer Software For Transient Flow Measurements," *Proceedings of the International Conference of Computers in Engineering,* ASME, 1985.

[11]Johnston, S.C., "Precombustion Fuel/Air Distributions in a Stratified Charge Engine Using Laser Raman Spectroscopy," SAE Paper 790433, 1979.

[12]Pitts, W.M. and Kashiwagi, T., "The Application of Laser-Induced Rayleigh Light Scattering to the Study of Turbulent Mixing." *Journal of Fluid Mechanics,* Vol. 141, 1984, pp. 391-429.

[13]Green, H.G., "Developments In Signal Analysis For Laser Rayleigh Scattering," Imperial College, Mechanical Engineering Department, FS/85/03, 1986, to be published in *Journal of Physics E.*

[14]Graham, S. C., Grant, A. J., and Jones, J. M., "Transient Molecular Concentration Measurements in Turbulent Flows Using Rayleigh Light Scattering," *AIAA Journal,* Vol. 12, Dec. 1974, pp. 1140-1142.

[15]Green, H.G. and Whitelaw, J.H., "Velocity and Concentration Characteristics of the Near Field of Round Jets," Imperial College, Mechanical Engineering Department, FS/85/2, 1986, to be published in *Journal of Fluid Mechanics.*

[16]Gutmark, E., Wolfshtein, M., and Wygnanski, I., "The Plane Turbulent Impinging Jet," *Journal of Fluid Mechanics,* Vol. 88, 1978, pp. 737-756.

[17]Amano, R.S. and Brandt, H., "Numerical Study of Turbulent Axisymmetric Jets Impinging on a Flat Plate and Flowing Into an Axisymmetric Cavity," *Journal of Fluids Engineering,* Vol. 106, 1984, pp. 410-417.